Research Paper

pH- and photothermal-driven multistage delivery nanoplatform for overcoming cancer drug resistance

Wenjing Huang[1*], Hao Zhao[1*], Jiangshan Wan[1], Yang Zhou[1], Qingbo Xu[1], Yanbing Zhao[1,2✉], Xiangliang Yang[1,2✉], Lu Gan[1,2✉]

1. National Engineering Research Center for Nanomedicine, College of Life Science and Technology, Huazhong University of Science and Technology, Wuhan 430074, China
2. Hubei Key Laboratory of Bioinorganic Chemistry and Materia Medica, Huazhong University of Science and Technology, Wuhan 430074, China

*These authors contributed equally to this work.

✉ Corresponding authors: E-mail: lugan@mail.hust.edu.cn (L. Gan), zhaoyb@mail.hust.edu.cn (Y. Zhao), yangxl@mail.hust.edu.cn (X. Yang).

Abstract

Reversing multidrug resistance (MDR) remains a big challenge in cancer therapy. Combining the hyperthermia and chemotherapy is a promising strategy for efficient cancer treatment with MDR reversal. Gold nanocages (GNCs) are an ideal photothermal (PTT)-chemotherapy integration platform due to their good photothermal conversion efficiency and the unique hollow interiors. However, insufficient tumor cell internalization and *in vivo* premature drug leakage restrict the anticancer activity of GNCs-based drug delivery systems.

Methods: pH low insertion peptide (pHLIP)- and thermoresponsive poly(di(ethylene glycol) methyl ether methacrylate-co-oligo(ethylene glycol) methyl ether methacrylate) polymer-conjugated GNCs were rationally constructed to load anticancer drug doxorubicin (DOX@pPGNCs). Tumor acidic environment-responsive tumor cell internalization, and near-infrared (NIR) laser-induced tumor accumulation, penetration and on-demand drug release were systematically examined.

Results: DOX@pPGNCs display good photothermal efficacy and thermoresponsive property. NIR laser irradiations at the tumor site significantly enhance tumor accumulation and penetration. Once DOX@pPGNCs reach the tumor site, the conformational transformation of pHLIP at the acidic tumor microenvironment contributes to the enhanced cellular internalization. Furthermore, NIR laser-triggered photothermal effects induce the shrinkage of thermoresponsive polymer, resulting in the opening of the pores of GNCs and a rapid intracellular DOX release to the nuclei. DOX@pPGNCs exhibit synergistic antitumor effect with MDR reversal *in vitro* and *in vivo*.

Conclusion: DOX@pPGNCs present strong potential to overcome MDR in cancer.

Key words: pHLIP, temperature-sensitive polymer, tumor cell targeting, tumor accumulation and penetration, on-demand drug release, multidrug resistance reversal

Introduction

Chemotherapy is widely used in the field of cancer therapy. Multidrug resistance (MDR) is one of the major obstacles in the failure of cancer chemotherapy [1]. Several mechanisms, including insufficient accumulation at tumors, decreased drug uptake, increased drug efflux, metabolic detoxification and DNA repair were reported to be involved in the MDR in cancer [2-4]. Reversing the drug resistance remains a big challenge in cancer therapy.

Hyperthermia as a non-invasive clinical treatment modality exhibits competitive advantages in overcoming MDR in cancer [5-7]. Hyperthermia not only enhances tumor vascular permeability to promote the delivery of anticancer drug to deep tumor tissues [8-10], but also increases the sensitivity

of resistant cancer cells to chemotherapeutic drugs by inhibiting the expression of efflux transporters such as multidrug resistance-associated protein 1 (MRP1) [7,11]. Therefore, combining the hyperthermia and chemotherapy is a promising strategy for efficient cancer treatment with MDR reversal [12]. Gold nanocages (GNCs) have been used as a good photothermal (PTT)-chemotherapy integration platform due to their unique hollow interior and porous wall structure, high photothermal conversion efficiency and excellent biocompatibility [13-15]. However, the insufficient tumor cell internalization and premature drug leakage limit the anticancer activity of GNCs-based drug delivery systems [16,17]. Although several strategies have been used to solve these problems, including conjugating GNCs with ligands that actively bind to surface receptors overexpressed in tumor cells to increase their tumor accumulation [18,19], and modification of GNCs with thermally responsive polymers to block the pore outlets to avoid the *in vivo* premature drug release [20,21], *et al*, some issues still remain in GNCs-based drug carriers. For example, the targeting ligand was not specific for cancer cells, which might result in the toxicity to normal cells [22]. Meanwhile, the targeting moieties on the surface of nanoparticles induce protein adsorption, thus affecting their circulation time and lowering their capacity to passively accumulate in tumors by enhanced permeation and retention (EPR) effects [22].

The pH low insertion peptide (pHLIP), a peptide of 36 amino acids, should be a good candidate to be used for the modification of nanoparticles for enhanced tumor cell internalization. pHLIP undergoes a conformational transition from random coil to α-helix in response to weakly acidic tumor microenvironment, allowing it to insert into tumor cell membranes with the C-terminus inside cells and the N-terminus outside cells [23,24]. In this paper, we constructed a GNCs-based PTT-chemotherapy integration platform to reverse MDR in cancer (**Figure 1**), in which GNCs were conjugated with a thermoresponsive poly(di(ethylene glycol) methyl ether methacrylate-*co*-oligo(ethylene glycol) methyl ether methacrylate) (PMEO₂MA-OEGMA) polymer (**Figure 1A**) and further modified with pH-sensitive pHLIP through Au-S bonds (denoted as pPGNCs), and the anticancer drug doxorubicin (DOX) was then highly loaded to pPGNCs (denoted as DOX@pPGNCs) using ammonium sulfate gradient method (**Figure 1B**). pHLIP endows DOX@pPGNCs to be efficiently internalized into cancer cells at the tumor acidic microenvironment (**Figure 1B-C**). As a new thermoresponsive polymer, PMEO₂MA-OEGMA shows better biocompatibility, more feasible and

sensitive thermoresponsiveness than poly(*N*-isopropylacrilamide), a well-known thermoresponsive polymer [25-27]. The hydrophilic nature of PMEO₂MA-OEGMA ensures long blood circulation time of GNCs by preventing the opsonization via the reticuloendothelial system. By changing the feeding ratio of two monomers in the polymerization process, the lower critical solution temperature (LCST) of PMEO₂MA-OEGMA could be rationally adjusted to ca. 41.6 °C, between the body temperature and hyperthermia temperature, thus serving as a temperature sensitive gate keeper. That is, the chains of PMEO₂MA-OEGMA polymer are extended at the body temperature, blocking the pore outlets of GNCs to avoid the premature drug release in blood circulation. When the temperature increases up to the LCST of PMEO₂MA-OEGMA owing to the NIR laser-triggered photothermal effects of GNCs at the tumor tissues, its chains shrink as temperature sensitive coil-granule conformation transition occurs, resulting in the opening of the pores of GNCs and a rapid intracellular drug release (**Figure 1B-C**). Meanwhile, NIR laser irradiation at the tumor tissues markedly improves tumor accumulation and penetration of DOX@pPGNCs (**Figure 1C**). The obtained DOX@pPGNCs efficiently surmount a series of physiological barriers of anticancer drug following systemic administration, achieving synergized thermo-chemotherapy and excellent antitumor effect in adriamycin-resistant tumor model.

Results and Discussion

Preparation and characterization of pPGNCs

To construct the temperature sensitive pHLIP-decorated GNCs, PMEO₂MA$_x$-OEGMA$_{200-x}$ polymer was firstly synthesized. It was known that the LCST of temperature-responsive copolymers could be adjusted by changing the ratio of the monomers [28]. Three polymers with different LCSTs that were PMEO₂MA₁₆₀-OEGMA₄₀, PMEO₂MA₁₂₀-OEGMA₈₀ and PMEO₂MA₈₀-OEGMA₁₂₀ (denoted as P$_L$OEG, POEG and P$_H$OEG, respectively) were synthesized by changing the molar ratio of MEO₂MA and OEGMA. The successful synthesis was confirmed by ¹H-NMR spectra (**Figure S1**). Gel permeation chromatography (GPC) analysis showed that the molecular weight of P$_L$OEG, POEG and P$_H$OEG were 41.1, 48.8 and 53.7 kDa (**Figure 2A, Figure S2A and Table S1**), consistent with their theoretic values. P$_L$OEG, POEG and P$_H$OEG exhibited the thermosensitive property and their LCSTs were calculated to be 31.6, 41.6 and 52.2 °C (**Figure 2B and Figure S2B**), respectively, suggesting that these polymers are hydrophilic and keep stretched chain

conformation below their LCST, while turning into hydrophobic and shrunken chain conformation as temperature raises to above their LCST.
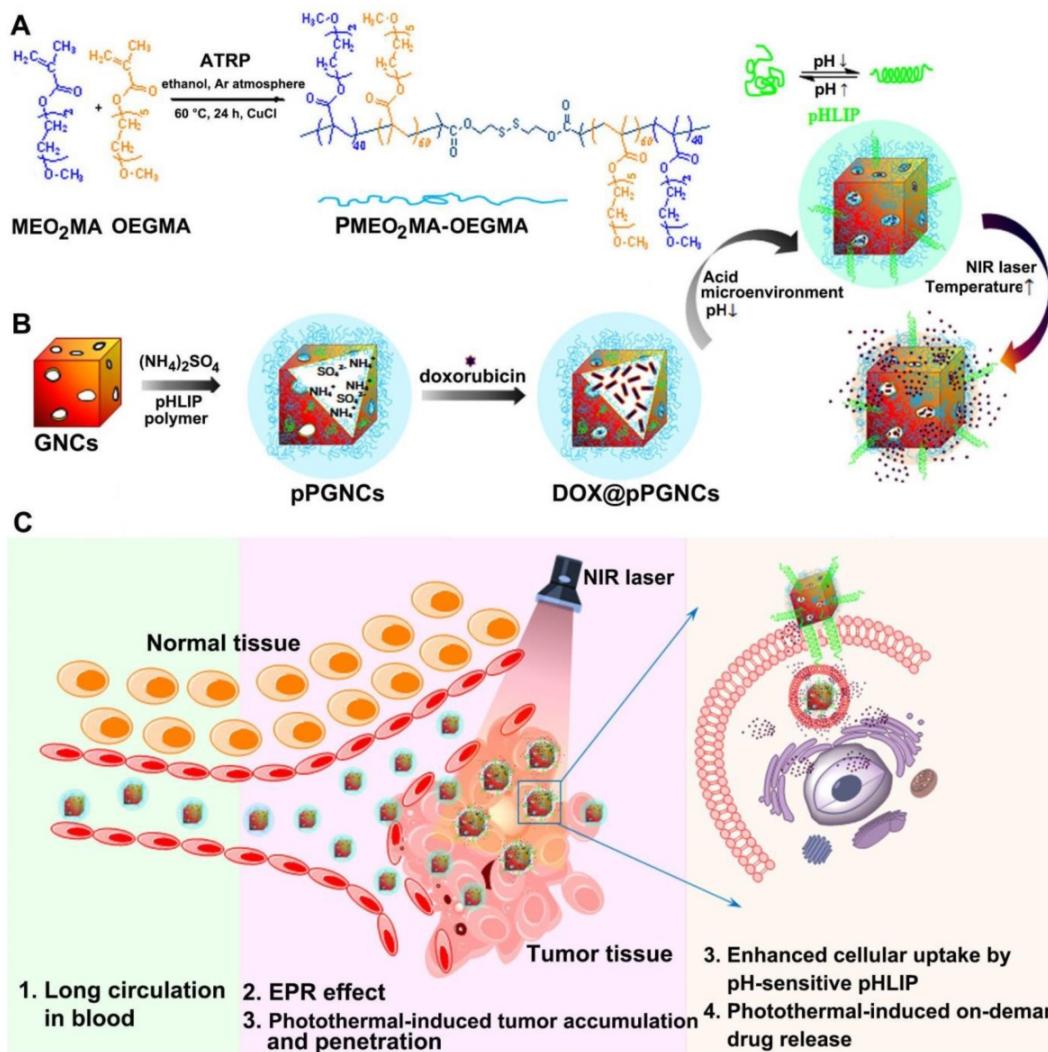
Figure 1. Schematic illustration of DOX@pPGNCs for synergistic PTT-chemotherapy to reverse MDR in cancer. **(A)** Synthesis of POEG. (B) Construction and characterization of DOX@pPGNCs. **(C)** Schematic illustration of the NIR laser-induced *in vivo* transport process of DOX@pPGNCs.
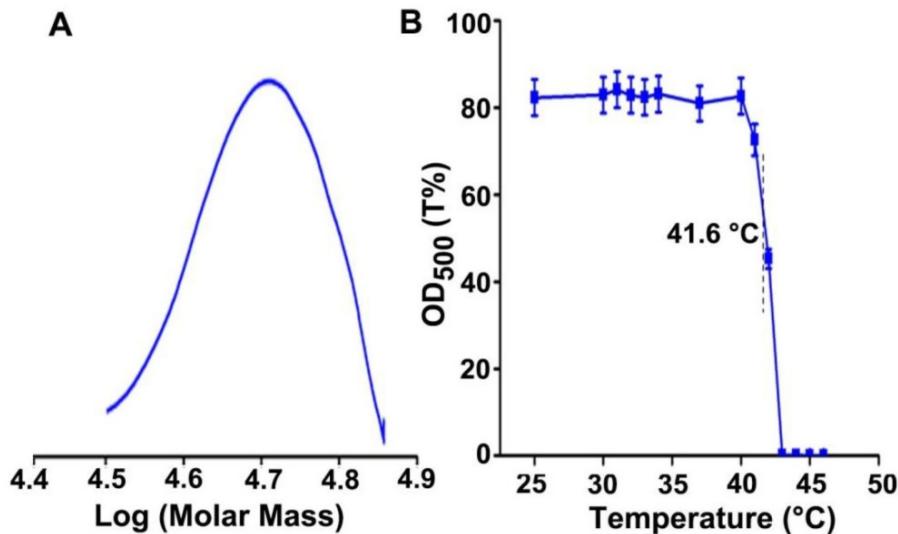
Figure 2. Characterization of POEG. **(A)** GPC spectrum of POEG. **(B)** Transmittance of POEG at 500 nm after incubation in PBS at the indicated temperatures for 5 min. The data are presented as the mean ± SD (n = 3).

Figure 3. Characterization of pPGNCs. **(A)** Microstructure and element composition of GNCs, PGNCs and pPGNC. **(B)** Fluorescence spectra of GNCs, pHLIP, PGNCs and pPGNCs at the excitation wavelength of 280 nm. **(C)** CD spectra of GNCs, pHLIP, PGNCs and pPGNCs. **(D)** TGA analysis of POEG, GNCs, PGNCs and pPGNCs. (E) Diameter change of GNCs and pPGNCs incubating in PBS at the different temperatures. The data are presented as the mean ± SD (n = 3).

Subsequently, GNCs were synthesized through galvanic replacement reaction using silver nanocube templates. PMEO$_2$MA-OEGMA$_2$-based polymer, including P$_L$OEG, POEG or P$_H$OEG, and pHLIP was anchored to GNCs through Au-S bonds to obtain PMEO$_2$MA-OEGMA- and pHLIP-decorated GNCs (denoted as pP$_L$GNCs, pPGNCs or pP$_H$GNCs, respectively). High-resolution transmission electron microscopy (HR-TEM) showed that GNCs, POEG-conjugated GNCs (denoted as PGNCs) and pPGNCs possessed cube-shaped morphology (**Figure 3A**). HR-TEM analysis in combination with STEM/energy dispersive X-ray (EDX) elemental mapping revealed that only oxygen and carbon elements were detected on PGNCs, while nitrogen, oxygen and carbon elements were detected on pPGNCs (**Figure 3A**). In contrast, no nitrogen, oxygen and carbon elements existed on bare GNCs (**Figure 3A**). These results indicated that both POEG and pHLIP were conjugated to GNCs in pPGNCs. Furthermore, fluorescence emission spectra analysis showed that the emission peak of pHLIP at 344 nm

was detected in pPGNCs (**Figure 3B**). In addition, there was no obvious difference in circular dichroism (CD) spectra of pHLIP and pPGNCs (**Figure 3C**). These results further confirmed that pHLIP was successfully anchored to GNCs and maintained its intact secondary structure after conjugation. Thermogravimetric analysis (TGA) of POEG, bare GNCs, PGNCs and pPGNCs revealed that 18.3% polymers and 5.9% pHLIP exhibited on pPGNCs (**Figure 3D**), indicating that there were about 42000 pHLIP molecules on a GNC particle.

To determine whether conjugation of PMEO$_2$MA-OEGMA and pHLIP to GNCs affected their thermoresponsive property, pPGNCs, pP$_L$GNCs or pP$_H$GNCs were incubated in PBS at different temperatures and their diameters were then determined by DLS analysis (**Figure 3E**). No significant change in the diameter of GNCs was detected at different temperatures. However, the diameter of pPGNCs remarkably decreased after incubation in PBS at above 42 °C, while their diameter returned from 140 to 160 nm after decreasing

temperature from 44 to 41 °C. These results suggested that pPGNCs preserved the thermosensitive property and POEG chains shrank on pPGNCs above its LCST of 41.6 °C. In contrast, the diameter of pP$_H$GNCs remained unchanged at temperatures from 25 to 44 °C (the LCST of P$_H$OEG was 52.2 °C), and the diameter of pP$_L$GNCs decreased from 30 to 33 °C and increased from 33 to 30 °C (the LCST of P$_L$OEG was 31.6 °C, **Figure S2C**).

NIR laser-triggered on-demand DOX release from DOX@pPGNCs

Anticancer drug DOX was then loaded into pPGNCs, pP$_L$GNCs or pP$_H$GNCs by ammonium sulfate gradient method [16,29]. Conjugation of POEG polymer increased the diameter and decreased the zeta-potential of GNCs (**Figure 4A**). However, DOX loading did not markedly affect the diameter and zeta-potential of pPGNCs (**Figure 4A**). UV-Vis-NIR spectra analysis showed that conjugation of POEG and pHLIP and loading DOX did not affect the absorption of GNCs. However, NIR laser irradiation increased DOX absorption of DOX@pPGNCs (**Figure S3**), suggesting that DOX was loaded into the hollow cavity of GNCs rather than adsorbing on the surface. Moreover, TEM analysis showed that there was no significant morphology change after DOX loading into pPGNCs (**Figure 4B**). The drug loading of pPGNCs was calculated to be 11.3%.
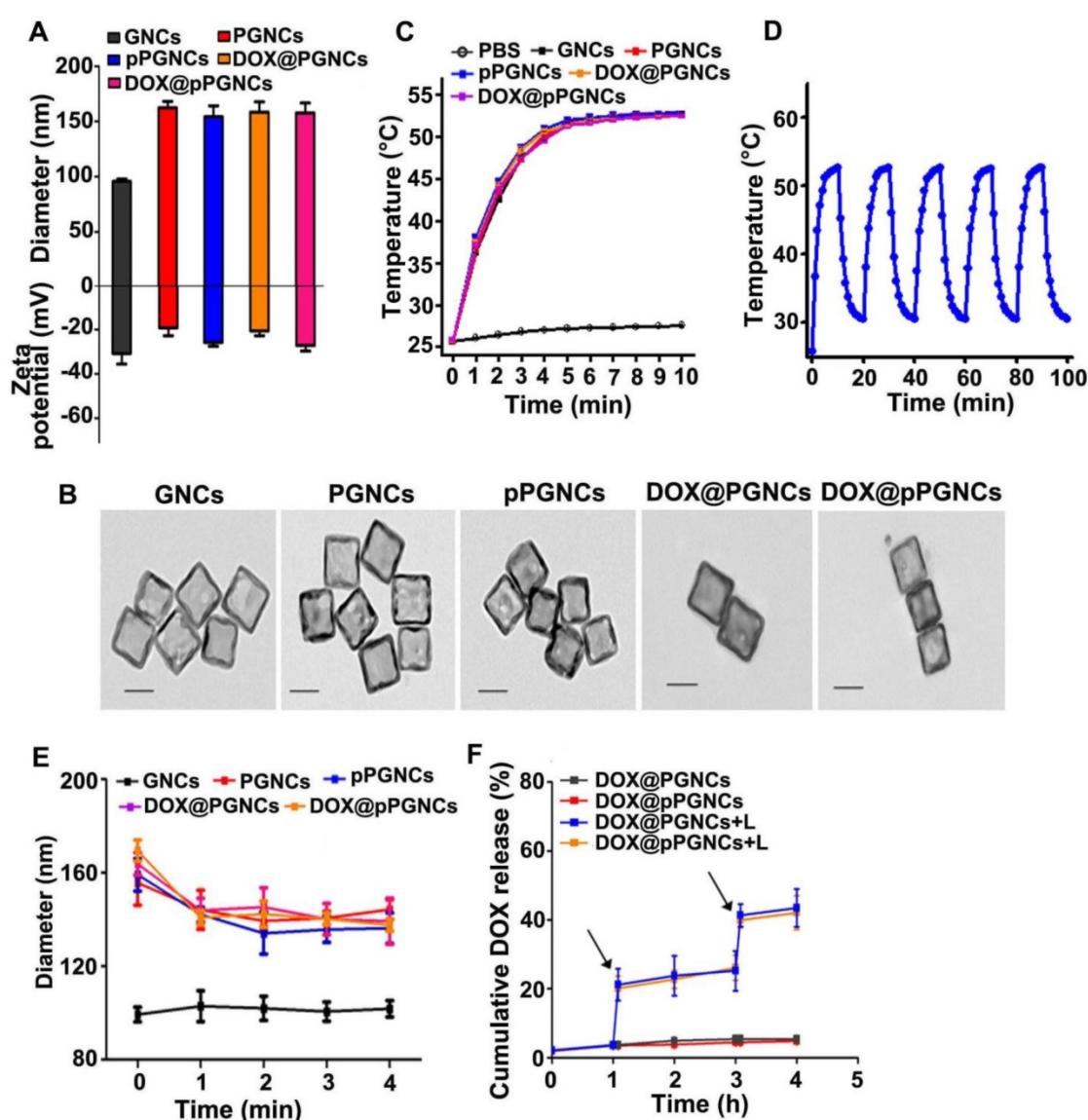
Figure 4. NIR laser-triggered photothermal drug release from DOX@pPGNCs. (A) Diameter and zeta potential of GNCs, PGNCs, pPGNCs, DOX@PGNCs and DOX@pPGNCs. **(B)** TEM images of GNCs, PGNCs, pPGNCs, DOX@PGNCs and DOX@pPGNCs. Scale bar: 50 nm. **(C)** Temperature of PBS, GNCs, PGNCs, pPGNCs, DOX@PGNCs and DOX@pPGNCs upon 808 nm laser irradiation (0.7 W/cm²) for different time intervals. **(D)** Photothermal stability of DOX@pPGNCs undergoing five cycles of 808 nm laser irradiation (0.7 W/cm²) and then cooling to room temperature. **(E)** Diameter of GNCs, PGNCs, pPGNCs, DOX@PGNCs and DOX@pPGNCs in response to 808 nm laser irradiation (0.7 W/cm²) for different time intervals. **(F)** *in vitro* DOX release profiles from DOX@PGNCs and DOX@pPGNCs in PBS with or without 808 nm laser irradiation (0.7 W/cm²) for 5 min. Black arrows indicate the irradiation points. The data are presented as the mean ± SD (n = 3).

To determine whether GNCs preserved photothermal effects after modification with POEG and pHLIP and the subsequent DOX loading, GNCs, PGNCs, pPGNCs, DOX@PGNCs and DOX@pPGNCs were irradiated with NIR laser (808 nm, 0.7 W/cm²) and their temperatures were then examined (**Figure 4C**). GNCs, PGNCs, pPGNCs, DOX@PGNCs and DOX@pPGNCs exhibited very similar temperature profiles. Their temperatures quickly increased up to 53 °C after irradiation for 5 min, although the temperature of PBS only increased to 27.5 °C after irradiation. These results revealed that POEG and pHLIP modification and DOX loading did not influence the photothermal activity of GNCs. Moreover, the temperature profile of DOX@pPGNCs upon NIR laser irradiation did not change even going through five irradiation-cooling cycles (**Figure 4D**). Meanwhile, NIR laser irradiation five times did not affect the morphology (**Figure S4**), size (**Figure S5A**), zeta potential (**Figure S5B**) and UV-Vis-NIR spectra (**Figure S3**) of DOX@pPGNCS, revealing their good photothermal stability.

To evaluate the effects of NIR laser-induced photothermal therapy on the characterization of DOX@pPGNCs, the diameter of DOX@pPGNCs was first measured upon NIR laser irradiation at 37 °C (**Figure 4E**). As expected, the diameter of PGNCs, pPGNCs, DOX@PGNCs and DOX@pPGNCs rapidly decreased after irradiation for 1 min, which was due to the shrinkage of POEG chains induced by NIR laser-triggered photothermal effects above their LCST. In contrast, NIR irradiation had no remarkable influence on the diameters of DOX@pP$_H$GNCs and DOX@pP$_L$GNCs (**Figure S6A**). The reason was that no phase-transition occurred for pP$_L$GNCs and pP$_H$GNCs during NIR irradiation, in which P$_L$OEG chains always collapsed on pP$_L$GNCs above its LCST and P$_H$OEG chains always stretched on pP$_H$GNCs below its LCST before and after NIR irradiation. These results suggested that the shrinkage of POEG upon NIR laser-induced photothermal effects might induce the pore opening of GNCs in DOX@pPGNCs, resulting in NIR laser-induced on-demand drug release.

To confirm NIR laser-triggered photothermal drug release from DOX@pPGNCs, the *in vitro* DOX release kinetics from DOX@pPGNCs was carried out in PBS with or without NIR laser irradiation (**Figure 4F**). Only 4.8% DOX was released within 4 h at 37 °C in the absence of NIR laser irradiation. However, the cumulative DOX release increased from 3.7 to 20.1% upon 808 nm laser irradiation for 5 min during 1 h. Furthermore, rapid DOX release was consistently observed upon 808 nm laser irradiation in another cycle. These results revealed that DOX@pPGNCs

were stable under physiological condition and precisely released drug upon NIR laser irradiation. In contrast, 76.7% DOX was released from DOX@pP$_L$GNCs and only 5.6% DOX was released from DOX@pP$_H$GNCs at 37 °C without NIR laser irradiation (**Figure S6B**). NIR laser irradiation did not significantly affect DOX release from DOX@pP$_L$GNCs and DOX@pP$_H$GNCs (**Figure S6B**). These results demonstrate that POEG function as a gatekeeper of GNCs to control NIR laser-triggered precise on-demand DOX release from DOX@pPGNCs.

Cellular uptake and synergistic cytotoxicity of DOX@pPGNCs *in vitro*

To determine the biological function of DOX@pPGNC, the cellular uptake of DOX@pPGNCs by sensitive human breast cancer MCF-7 cells and adriamycin-resistant MCF-7 (MCF-7/ADR) cells was evaluated. MCF-7 or MCF-7/ADR cells were incubated with DOX@PGNCs or DOX@pPGNCs at pH 7.4 or 6.5 for 4 h and then the intracellular Au contents were determined by graphite furnace atomic absorption spectrometry (**Figure 5A-B**). There was no significant difference in cellular uptake of DOX@PGNCs and DOX@pPGNCs by MCF-7 and MCF-7/ADR cells at pH 7.4. However, significantly enhanced intracellular accumulation of DOX@pPGNCs was detected in MCF-7 and MCF-7/ADR cells at pH 6.5 compared with DOX@PGNCs. Similar results were also found in human hepatocellular carcinoma HepG2 cells and adriamycin-resistant HepG2/ADM cells (**Figure 5C-D**). These results suggest that pHLIP coating increased the cellular uptake of DOX@pPGNCs by cancer cells under acidic pH environment. The reason might be that the increase in α-helix content of pHLIP at acidic pH environment contributed to the enhanced cellular uptake of DOX@pPGNCs, as evidenced by the more α-helix content (**Figure S7A and Table S2**) and correspondingly more cellular internalization (**Figure S7B**) of DOX@pPGNCs at acidic pH values. Macropinocytosis-, caveolin- and clathrin-medicated endocytosis was involved in the internalization of DOX@pPGNCs and DOX@PGNCs (**Figure S8**).

To investigate the synergistic anticancer activity of DOX@pPGNCs from photothermal therapy of GNCs and DOX chemotherapy, MCF-7 or MCF-7/ADR cells were treated with free DOX, GNCs, PGNCs, pPGNCs, DOX@PGNCs or DOX@pPGNCs for 24 h, followed with or without 808 nm laser irradiation for 5 min, the *in vitro* cytotoxicity was then evaluated by MTT assay (**Figure 5E-F**). Free DOX induced stronger cytotoxicity against MCF-7 cells than MCF-7/ADR cells, confirming the drug resistance of MCF-7/ADR cells. NIR laser irradiation
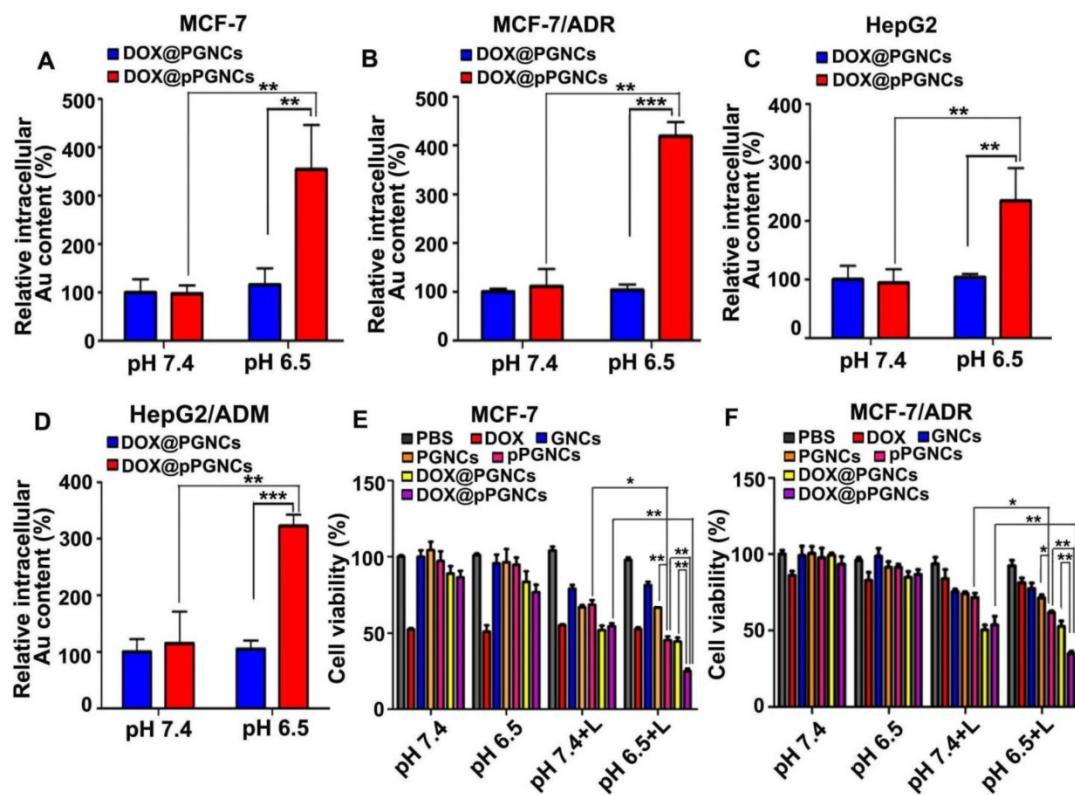
Figure 5. Cellular uptake and *in vitro* cytotoxicity of DOX@pPGNCs. (A-D) Intracellular Au content in MCF-7 **(A)**, MCF-7/ADR **(B),** HepG2 **(C)** and HepG2/ADM cells **(D)** after treatment with DOX@PGNCs or DOX@pPGNCs at Au concentration of 10 μg/mL for 12 h at pH 7.4 or 6.5, respectively. **(E-F)** *in vitro* cytotoxicity against MCF-7 (E) or MCF-7/ADR cells (F) after treatment with PBS, free DOX, GNCs, PGNCs, pPGNCs, DOX@PGNCs or DOX@pPGNCs at DOX concentration of 1.2 μg/mL and Au concentration of 10 μg/mL at pH 7.4 or 6.5 for 24 h, respectively, followed with or without 808 nm laser irradiation (0.7 W/cm²) for 5 min and incubation for another 4 h. The data are presented as the mean ± SD (n = 3).

significantly increased the cytotoxicity of PGNCs and pPGNCs against MCF-7 and MCF-7/ADR cells at both pH 7.4 and 6.5. Meanwhile, DOX@PGNCs and DOX@pPGNCs further enhanced the cytotoxicity against MCF-7 and MCF-7/ADR cells in response to NIR laser irradiation compared with PGNCs and pPGNCs, suggesting the synergistic effects of thermo-chemotherapy. However, the cytotoxicity of pPGNCs and DOX@pPGNCs against MCF-7 and MCF-7/ADR cells upon NIR laser irradiation at pH 6.5 was stronger than that at pH 7.4. DOX@pPGNCs exhibited the strongest cytotoxicity against MCF-7 and MCF-7/ADR cells upon NIR laser irradiation at pH 6.5. These results confirmed that pHLIP conjugation increased the internalization of DOX@pPGNCs into cancer cells under tumor acidic microenvironment, and DOX@pPGNCs upon NIR laser irradiation could generate effective synergistic thermo-chemotherapy with MDR reversal.

NIR Laser-Induced Intracellular Drug Release of DOX@pPGNCs

In view that NIR laser induced on-demand anticancer drug release from DOX@pPGNCs, the intracellular drug release of DOX@pPGNCs upon NIR laser irradiation was determined in MCF-7/ADR

cells. MCF-7/ADR cells were treated with DOX@PGNCs or DOX@pPGNCs for 4 h at pH 7.4 or 6.5, washed with PBS, and then irradiated with 808 nm laser for 5 min. Intracellular DOX fluorescence was detected by confocal microscope and flow cytometry. Confocal microscopic images showed that NIR laser irradiation increased the intracellular DOX fluorescence of DOX@PGNCs and DOX@pPGNCs at both pH 7.4 and 6.5 (**Figure 6A**), revealing the NIR laser-induced photothermal effects resulted in intracellular drug release from DOX@pPGNCs. However, no significant difference was detected in DOX@PGNCs-treated group upon NIR laser irradiation at pH 7.4 and 6.5, while stronger intracellular DOX fluorescence and more DOX nuclear translocation were found in DOX@pPGNCs-treated group in response to NIR irradiation at pH 6.5 than that at pH 7.4, even better than DOX@PGNCs-treated group upon NIR irradiation at pH 6.5 (**Figure 6A**). The qualitative results from confocal microscope were further confirmed by the quantitative results obtained from flow cytometry (**Figure 6B-C**). These results further revealed that pHLIP coating increased the cellular uptake of DOX@pPGNCs under tumor acidic microenvironment, and DOX was efficiently released

and then translocated to nucleus in response to NIR laser-induced photothermal effects.

NIR laser-induced tumor accumulation and penetration of DOX@pPGNCs

It has been widely acknowledged that *in vivo* biodistribution of anticancer drugs affects their therapeutical efficacy and potential side effects [30,31]. To detect the biodistribution of DOX@pPGNCs, MCF-7/ADR tumor-bearing nude mice were intravenously injected with free DOX, DOX@PGNCs or DOX@pPGNCs, followed with or without 808 nm laser irradiation for 5 min. At 24 h after administration, the mice were executed, and DOX contents in major organs (heart, liver, spleen, lung and kidney) and tumors were determined. As shown in **Figure 7A**, DOX@pPGNCs and DOX@PGNCs with or without NIR laser irradiation

exhibited nearly 2 fold lower DOX accumulation in the heart tissues than free DOX, indicating that DOX@pPGNCs and DOX@PGNCs might have ability to reduce DOX cardiotoxicity compared with free DOX. Conversely, DOX content in tumor tissues of mice treated with DOX@PGNC was nearly 1.8 times of free DOX, which might be due to EPR effects of DOX@PGNCs. However, DOX@pPGNCs exhibited the highest DOX accumulation in tumors compared with DOX@PGNCs and DOX due to the enhanced tumor cell internalization of pHLIP. Moreover, DOX accumulation of DOX@PGNCs and DOX@pPGNsC in the tumors enhanced significantly upon irradiation with NIR laser, revealing that NIR laser-induced photothermal effects of GNCs further increased their tumor accumulation.
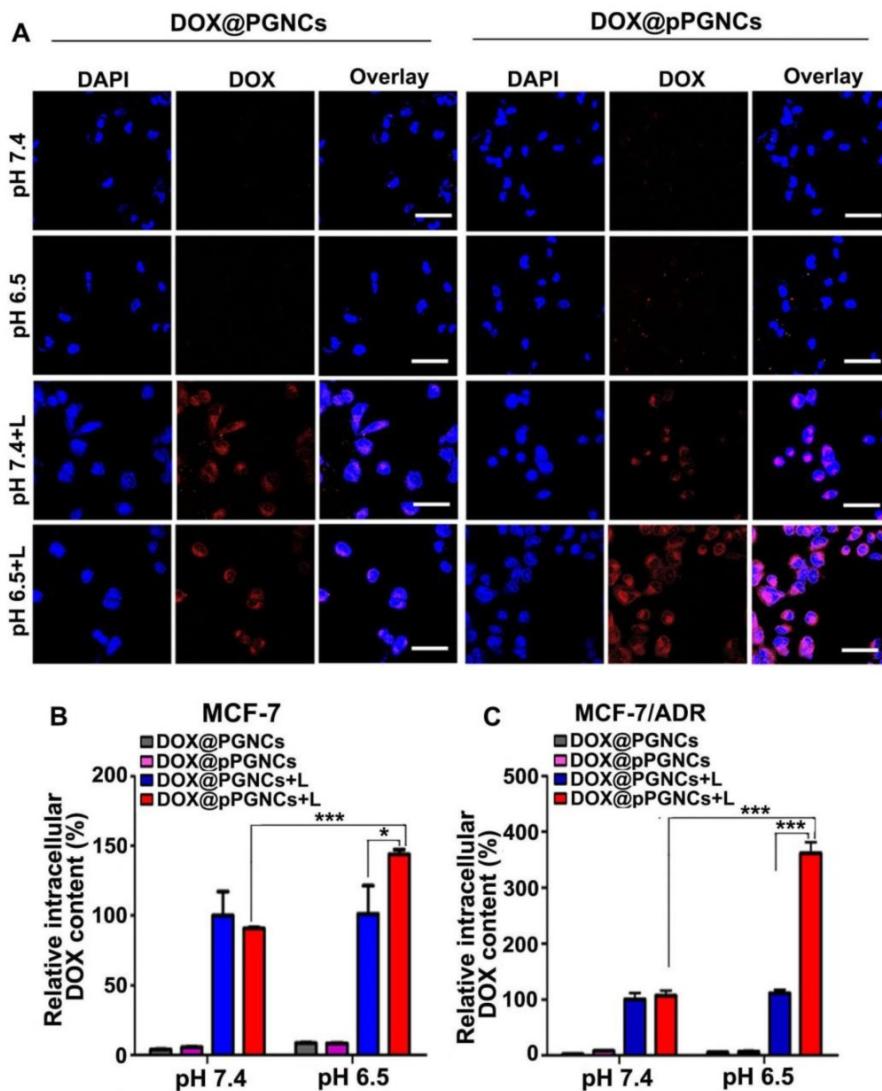
Figure 6. NIR laser-triggered intracellular DOX release from DOX@pPGNCs. (A) Confocal microscopic images of MCF-7/ADR cells after treatment with DOX@PGNCs or DOX@pPGNCs at DOX concentration of 2 μg/mL for 4 h at pH 7.4 or 6.5, respectively, followed with or without 808 nm NIR laser irradiation (0.7 W/cm²) for 5 min. Scale bar: 50 μm. **(B, C)** Intracellular DOX content in MCF-7 (B) and MCF-7/ADR cells **(C)** after treatment with DOX@PGNCs or DOX@pPGNCs at DOX concentration of 2 μg/mL for 4 h at pH 7.4 or 6.5, respectively, followed with or without 808 nm NIR laser irradiation (0.7 W/cm²) for 5 min by flow cytometry. The data are presented as the mean ± SD (n = 3). *$P<0.05$, ***$P<0.001$.
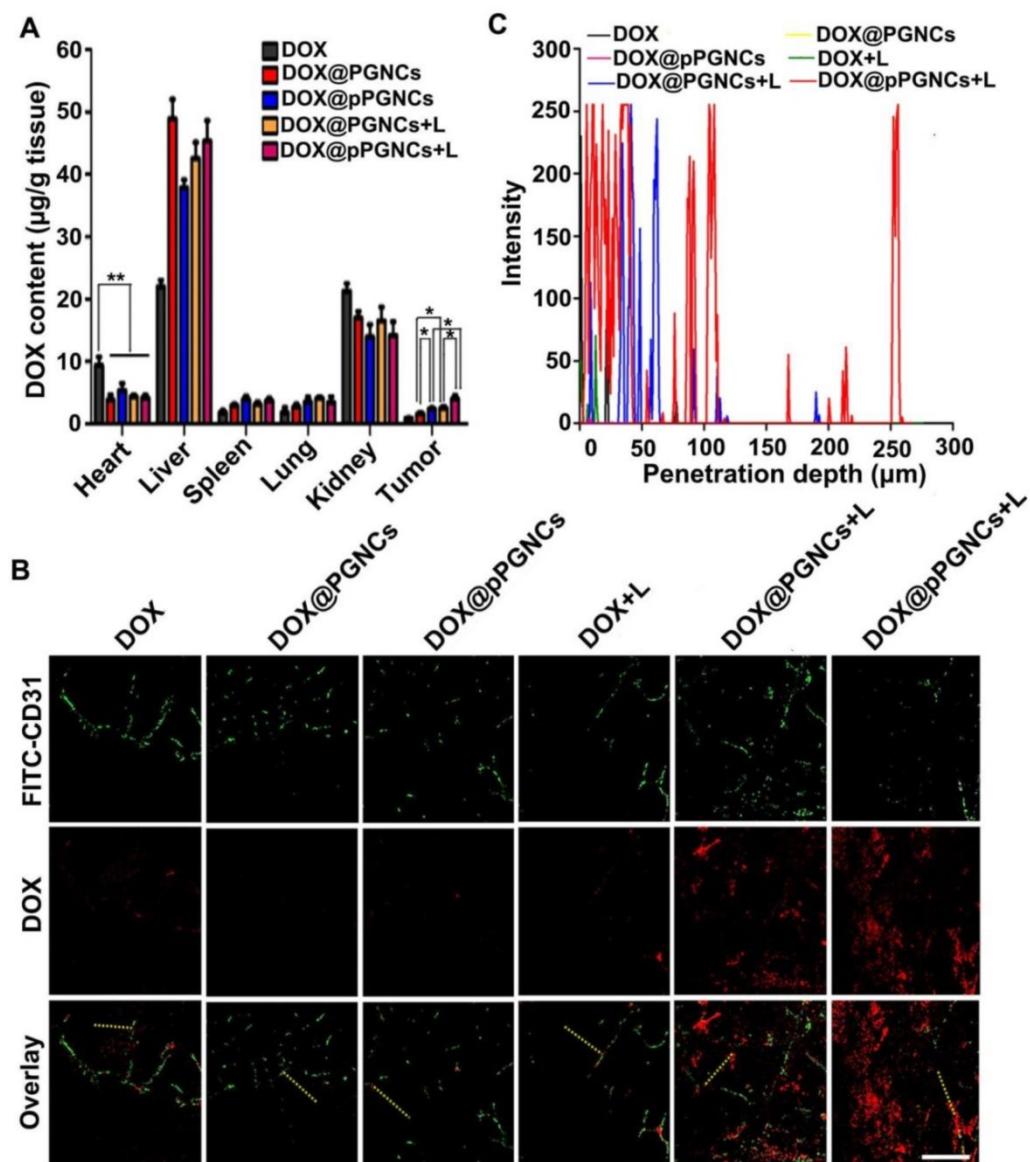
Figure 7. NIR laser-induced tumor accumulation and deep tumor penetration in MCF-7/ADR tumor-bearing nude mice. (A) DOX content in tumor and major organs including heart, liver, spleen, lung and kidney of MCF-7/ADR tumor-bearing mice at 24 h after intravenous injection of free DOX, DOX@PGNCs or DOX@pPGNCs at 2.4 mg DOX/kg dosage, followed with or without 808 nm laser irradiation (0.7 W/cm²) for 5 min. The data are presented as the mean ± SD (n = 3 mice for each group). *P<0.05, **P<0.01. **(B, C)** Colocalization of free DOX, DOX@PGNCs or DOX@pPGNCs (red) with FITC-CD31 antibody labeled endothelial cells (green) in tumor sections of MCF-7/ADR tumor-bearing mice at 24 h after intravenous administration of free DOX, DOX@ING or DOX@pPGNCs at 2.4 mg DOX/kg dosage, followed with or without 808 nm laser irradiation (0.7 W/cm²) for 5 min. scale bar is 50 μm. **(C)** The distribution of DOX fluorescence from tumor blood vessels to tumor tissues on the specified yellow line in B (n = 3 mice for each group).

Due to the abnormal vascular structure, increased interstitial fluid pressure and compact extracellular matrix in tumor tissues, nanoparticles are majorly accumulated near the tumor blood vessels, thus decreasing the opportunity of delivering anticancer drugs to cancer cells [32-34]. Improving the tumor penetration capacity of nanoparticles was crucial for increasing the therapeutic efficacy. To evaluate their tumor penetration ability, MCF-7/ADR tumor-bearing nude mice were intravenously injected with free DOX, DOX@PGNCs or DOX@pPGNCs, followed with or without 808 nm laser irradiation for 5 min. At 24 h after injection, DOX fluorescence in tumor sections was evaluated by confocal microscope

(**Figure 7B-C**). Consistent with the tumor accumulation data, NIR laser irradiation significantly increased DOX fluorescence in tumors of DOX@PGNCs- and DOX@pPGNCs-treated mice, and DOX@pPGNCs exhibited the strongest DOX fluorescence in tumors upon NIR laser irradiation, confirming that pHLIP coating increased tumor accumulation of DOX@pPGNCs and NIR laser irradiation further increased their tumor accumulation. Meanwhile, compared with other group, DOX fluorescence was scattered throughout the entire tumor section in DOX@pPGNCs-treated mice in the presence of NIR laser irradiation, rarely colocalized with fluorescein isothiocyanate isomer I

(FITC)-labeled CD31, a blood vasculature endothelial cell marker. These results revealed that NIR laser induced excellent tumor penetration ability of DOX@pPGNCs.

In vivo photothermal effects of DOX@pPGNCs

In view of the enhanced tumor accumulation of DOX@pPGNCs, the *in vivo* phototheraml effects were measured in MCF-7/ADR tumor-bearing nude mice (**Figure 8A-B**). The mice were intravenously administrated with free DOX, GNCs, PGNCs, pPGNCs, DOX@PGNCs or DOX@pPGNCs. At 24 h after administration, the tumor tissues were irradiated with NIR laser for different time intervals and their temperature was detected by an IR camera. Consistently, the irradiated tumor tissues of pPGNCs- and DOX@pPGNCs-treated mice exhibited a significant temperature increase compared with those of GNCs-, PGNCs- and DOX@PGNCs-treated mice, which might be due to their enhanced tumor accumulation capacity. The maximal temperature of the irradiated tumor tissues in pPGNCs- and DOX@pPGNCs-treated mice can reach 49.6 °C, high enough to kill cancer cells. However, the temperature only increased by about 3 °C in the irradiated tumors of free DOX-treated mice.

In vivo synergistic thermo-chemotherapeutic activity of DOX@pPGNCs in MCF-7/ADR tumor-bearing mice

Considering NIR laser-induced elevated temperature for photothermal therapy and enhanced DOX accumulation and penetration in tumor tissues, cellular uptake by cancer cells and on-demand intracellular drug release, the *in vivo* anticancer activity of DOX@pPGNCs was evaluated in MCF-7/ADR tumor-bearing nude mice (**Figure 9A**), intravenous injection of free DOX did not induce significant tumor inhibition, confirming the successful construction of drug-resistant tumor model. NIR laser irradiation did not affect the anticancer efficacy of DOX, suggesting that NIR laser itself did not generate the photothermal anticancer activity. Even though PGNCs and pPGNCs achieved enhanced anticancer activity upon NIR laser irradiation, the anticancer activity of pPGNCs upon NIR laser irradiation was stronger than PGNCs upon NIR irradiation, which was due to the enhanced tumor accumulation after pHLIP coating. DOX@pPGNCs exhibited the strongest anticancer activity with a tumor inhibition rate of 97.3% (2 mice undergoing tumor ablation in 5 mice), suggesting the synergistic effects of thermo-chemotherapy in drug-resistant MCF-7/ADR tumor-bearing mice. The tumor weight excised at the end of treatment also showed the same trend (**Figure 9B-C**).
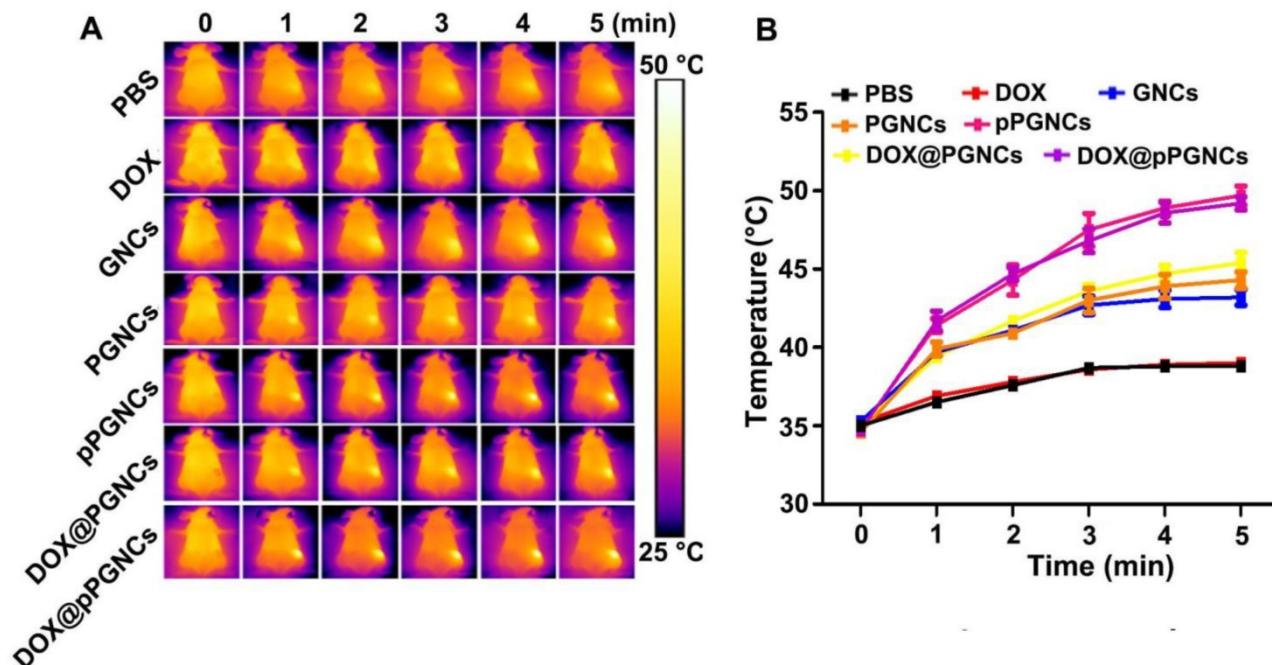
Figure 8. *in vivo* **photothermal effects of DOX@pPGNCs. (A)** NIR laser-triggered temperature images of tumors recorded by an IR camera at 24 h after MCF-7/ADR tumor-bearing nude mice were intravenously injected with PBS, free DOX, GNCs, PGNCs, pPGNCs, DOX@PGNCs or DOX@pPGNCs at the Au dosage of 20 mg/kg, followed with 808 nm laser irradiation (0.7 W/cm²) for different time intervals. The data are presented as the mean ± SD (n = 3 mice for each group).
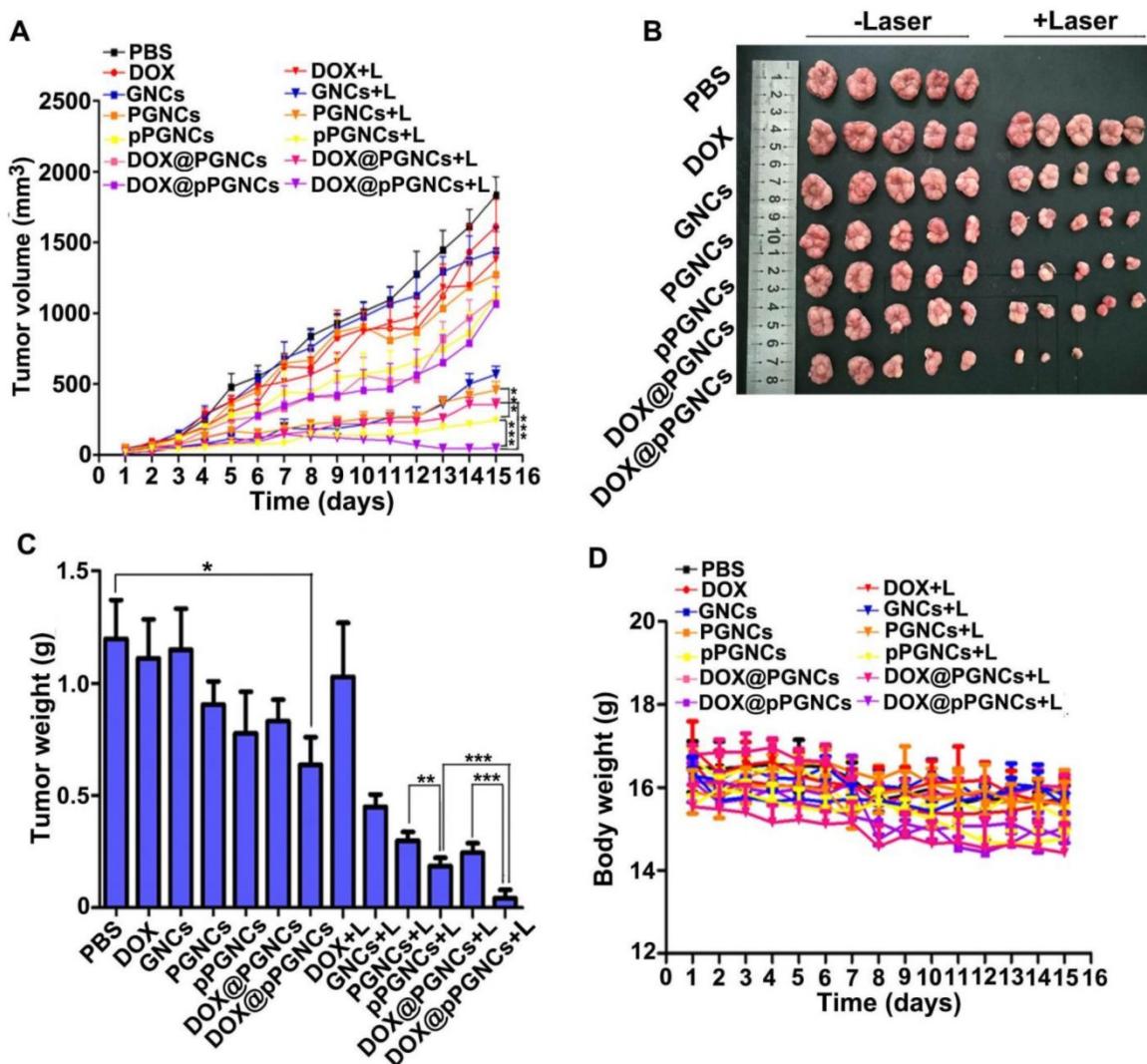
Figure 9. *In vivo* **anticancer activity of DOX@pPGNCs. (A)** Tumor growth curves of MCF-7/ADR tumor-bearing nude mice after intravenous injection of various formulations at the dosage of 20 mg/kg Au and 2.4 mg/kg DOX, followed with 808 nm laser irradiation (0.7 W/cm²) for 5 min at the tumor sites once every other day. **(B)** Photos of tumors after treatment. **(C)** Tumor weight after treatment. **(D)** Body weight change of MCF-7/ADR tumor-bearing nude mice after treatment as above. The data are presented as the mean ± SD (n = 5 mice for each group). $**P<0.01$, $***P<0.001$.

To test the biosafety of DOX@pPGNCs, body weight, an important indicator of general systemic toxicity, was evaluated during treatment. No significant difference in body weight was found in mice administrated with free DOX, DOX@PGNCs or DOX@pPGNCs with or without NIR laser irradiation (**Figure 9D**). Meanwhile, the histopathological examinations of the major organs were performed by H&E staining (**Figure S9**). All treatment groups did not show obvious pathological changes in heart, liver, spleen, lung and kidney. These results revealed that DOX@pPGNCs were capable of overcoming MDR and exhibited stronger anticancer activity with few adverse effects.

Conclusions

In summary, we have successfully fabricated thermoresponsive POEG- and pH-sensitive pHLIP-conjugated GNCs for DOX delivery to reverse MDR in cancer. DOX@pPGNCs display good photothermal efficacy and on-demand drug release. NIR laser-trigged photothermal effects induce the enhanced tumor accumulation and penetration of DOX@pPGNCs. After accumulation at tumor sites, DOX@pPGNCs are efficiently internalized into drug-resistant cancer cells by responding to the acidic tumor microenvironment. DOX@pPGNCs are stable in the blood circulation, while NIR laser irradiation at the tumor sites contributes to the shrinkage of POEG and facilitates the intracellular DOX release to enter into the nuclei, exhibiting the synergistic photothermal and chemotherapeutic cytotoxicity against drug-resistant cancer cells. Therefore, excellent *in vivo* tumor inhibition efficacy of DOX@pPGNCs was achieved in MCF-7/ADR tumor-bearing mice with no obvious side effects. This

finding provides a new synergistic strategy to acquire the ideal therapeutic effects in cancer treatment with MDR reversal.

Materials and Methods

Materials

MEO$_2$MA, OEGMA, bis[2-(2′-broMoisobutyryl-oxy)-ethyl]disulfide (BiBOEDS), silver trifluoroacetate (CF$_3$COOAg) and poly(vinylpyrrolidone) (PVP, M$_w$=55kD) were obtained from Sigma-Aldrich Corp (St Louis, MO, USA). Tris(2-dimethyl-aminoethyl)-amine (Me$_6$TREN) and anhydrous sodium hydrosulfide (NaHS) were purchased from Alfa Aesar (Shanghai, China). Ethylene glycol (EG, purity>99.0%), cuprous chloride (CuCl), chloroauric acid hydrate (HAuCl$_4$·4H$_2$O, Au content>47.8%) and 4′6-diamidino-2-phenylindole (DAPI) were purchased from Sinopharm Chemical Reagent Co., Ltd (Beijing, China). DMEM, RPMI 1640 and fetal bovine serum (FBS) were obtained from Gibco BRL/Life Technologies (Grand Island, NY, USA). pHLIP (ACEQNPIYWARYADWLFTTPLLLLDLALLVDADEGT) was synthesized by Bankpeptide Inc. (Heifei, China). All other reagents were of analytical grade and used without any further purification.

Synthesis of GNCs

GNCs were synthesized through galvanic replacement reaction between Ag nanocubes and HAuCl$_4$ [16,35]. Briefly, Ag nanocubes were first synthesized as follows. 50 mL of ethylene glycol was heated in 150 °C oil-bath for 30 min. Then 0.6 mL of NaHS solution in ethylene glycol (0.3 mM) was mixed into hot ethylene glycol under vigorous stirring, followed by mixing 12.5 mL of PVP solution in ethylene glycol (20 mg/mL), 5 mL of HCl solution in ethylene glycol (3.0 mM) and 4.0 mL of CF$_3$COOAg solution in ethylene glycol (282 mM). The reaction lasted for 45 min at 150 °C. The obtained Ag nanocubes were washed with acetone and deionized water to remove PVP and ethylene glycol. Subsequently, the refined Ag nanocubes were dispersed in deionized water.

Afterwards, 10 mL of Ag nanocubes (6.7 mM) was added to 90 mL of deionized water containing PVP (1.6 mg/mL) and heated to 90 °C for 10 min under vigorous stirring. Then 1.0 mM HAuCl$_4$ solution was added using a micro-infusion pump (WZ-50C6, Zhejiang Smiths Medical Instrument Co, Ltd, China) at 42 mL/h of injection rate until the solution had an localized surface plasmon resonance (LSPR) peak at 808 nm measured by UV-Vis-NIR spectroscopy (TU 1901, Beijing Tongyong General Instrumental Co, Ltd., Beijing, China). The crude

GNCs were collected by centrifugation at 10,000 rpm for 10 min and washed with ammonium hydroxide, absolute ethyl alcohol and deionized water, respectively. The refined GNCs were dispersed in deionized water and stored at 4 °C for further use.

Preparation of PMEO$_2$MA$_x$-OEGMA$_{200-x}$ with different LCSTs

PMEO$_2$MA$_x$-OEGMA$_{200-x}$ (polymerization degree x=160, 120 or 80) with different LCSTs were synthesized according to atom transfer radical polymerization (ATRP) [36]. Taking x = 120 for example, MEO$_2$MA (5.53 mL, 30 mmol), OEGMA (5.71 mL, 20 mmol) and absolute ethanol (10 mL) were mixed in a Schlenk tube under vigorous stirring. The reaction system was sequentially frozen by liquid nitrogen, vacuumed by a vacuum pump and argon-filling for one cycle. Afterwards, BiBOEDS (76 μL, 0.25 mmol) and Me$_6$TREN (135 μL, 0.5 mmol) were added into the Schlenk tube under argon atmosphere. After two cycles of liquid nitrogen refrigeration, vacuum and argon-filling, CuCl (50 mg, 0.5 mmol) was added into the solvents to initiate ATRP polymerization. After reacting at 60 °C for 24 h, PMEO$_2$MA$_x$-OEGMA$_{200-x}$ was obtained. The crude PMEO$_2$MA$_x$-OEGMA$_{200-x}$ was transferred to dialysis bag (MWCO: 3500 Da) against deionized water for 3 days to remove the small molecular impurities. Eventually, the refined PMEO$_2$MA$_x$-OEGMA$_{200-x}$ was freeze-dried and stored in a vacuum desiccator for further use. The molecular structure and molar mass of PMEO$_2$MA$_x$- OEGMA$_{200-x}$ were measured by ^{1}H-NMR spectrometer (600 MHz, AV400, Bruker, Switzerland) using CDCl$_3$ as solvent and GPC (1100 LC/MSD Trap, Agilent, USA) using 0.1 mM sodium nitrate aqueous solution as eluent, respectively. The temperature-transmittance curve of PMEO$_2$MA$_x$-OEGMA$_{200-x}$ (2 mg/mL, in PBS buffer) was determined by UV-Vis spectrophotometer (UV-3600, Shimadzu, Japan) at a wavelength of 500 nm in the temperature range of 25 – 50 °C. Their LCST was calculated by taking the derivative with respect to Boltzmann fitting of the temperature-transmittance curve.

Preparation of PMEO$_2$MA$_{120}$-OEGMA$_{80}$- and pHLIP-conjugated GNCs

GNCs were sequentially decorated with temperature-sensitive PMEO$_2$MA$_{120}$-OEGMA$_{80}$- and the N-terminus of the pHLIP. Briefly, 10 mL of PMEO$_2$MA$_{120}$-OEGMA$_{80}$ (50 mg/mL) was added dropwise to 1 mL of GNCs solution (10 mg/mL) under vigorous stirring. After reacting at room temperature for 3 days, the obtained PMEO$_2$MA$_{120}$-OEGMA$_{80}$-conjugated GNCs (denoted as PGNCs)

were collected by centrifugation at 10,000 rpm for 10 min and washed with deionized water. Then, the PGNCs were re-dispersed in 1 mL of deionized water. 5 mL of pHLIP (2 mg/mL) was added dropwise to the dispersion and the reaction was maintained for another 24 h. PMEO$_2$MA$_{120}$-OEGMA$_{80}$- and pHLIP-conjugated GNCs (denoted as pPGNCs) were collected by centrifugation at 10,000 rpm for 10 min, washed with deionized water and stored at 4 °C for further use.

Remote loading DOX into PGNCs and pPGNCs

DOX was loaded into PGNCs and pPGNCs by ammonium sulfate gradient method [15,28]. First, 0.5 mL of PGNCs and pPGNCs (10 mg/mL) were dispersed in 5.0 mL of ammonium sulfate solution (0.2 M) at 55 °C for 12 h. After 10 min of ultrasonic concussion, the dispersions were centrifuged at 12,000 rpm for 10 min at 4 °C and washed with deionized water for 3 times to remove unloaded ammonium sulfate. Afterwards, 2 mL of DOX solution (5 mg/mL) was added to ammonium sulfate-loaded PGNCs and pPGNCs and incubated at 4 °C for 12 h. DOX@PGNCs and DOX@pPGNCs were collected by centrifugation at 12,000 rpm for 10 min and washed with deionized water. The drug loading capacity (DLC) was calculated as the following equation: DLC%= ($W_{\text{administered DOX}}$-$C_f V_f$/$W_{\text{pPGNCs}}$)×100, where $W_{\text{administered DOX}}$ is the feeding amount of DOX, C_f and V_f are the concentration and volume of free DOX not being encapsulated into pPGNCs, and W_{pPGNCs} is the amount of pPGNCs.

Characterization

The element distribution mapping of GNCs, PGNCs and pPGNCs was evaluated by HR-TEM (300 kV, Tecnai G2 F30, FEI Corp, USA). The fluorescence spectra of pHLIP, GNCs, PGNCs and pPGNCs were measured by fluorescence spectrophotometer (F4500, Hitachi Co., Japan). The CD spectra of different formulations were measured at room temperature using a CD spectrometer (J-810, Jasco, Japan). TGA of different formulations was conducted on the Diamond TG/DTA (PerkinElmer Instruments Co. Ltd., USA) from room temperature to 600 °C at a heating rate of 10 °C/min. The hydrodynamic diameter and zeta potential of GNCs, PGNCs, pPGNCs, DOX@PGNCs and DOX@pPGNCs at Au concentration of 10 µg/mL were determined by dynamic light scattering (DLS, Zetasizer Nano ZS90, Malvern Instruments Ltd, UK) equipped with 4 mW He-Ne laser source (λ = 633 nm, scattering angle 90 °) in deionized water. The UV-Vis-NIR spectra of GNCs, PGNCs, pPGNCs, DOX@PGNCs and DOX@pPGNCs

were monitored by UV-Vis-NIR spectroscopy (TU 1901, Beijing Tongyong General Instrumental Co, Ltd., Beijing, China). The morphology of different formulations was determined by TEM (200 kV, Tecnai G2 20, FEI Corp., Netherlands).

In vitro photothermal effects

PBS, GNCs, PGNCs, pPGNCs, DOX@PGNCs or DOX@pPGNCs dispersions in PBS at Au concentration of 10 µg/mL were irradiated with 808 nm laser at a power density of 0.7 W/cm² for different time intervals. The temperature was measured by an FLIR E50 IR camera (FLIR Systems Inc., USA).

In vitro photothermal stability

DOX@pPGNCs dispersions in PBS at Au concentration of 10 µg/mL were irradiated with 808 nm laser at a power density of 0.7 W/cm² for 10 min and then cooled at room temperature for 10 min. The irradiation-cooling cycles were repeated for five times and the temperature was measured by an FLIR E50 IR camera.

In vitro NIR laser-induced DOX release

DOX@PGNCs or DOX@pPGNCs dispersions at Au concentration of 10 µg/mL were irradiated with or without 808 nm laser at a power density of 0.7 W/cm² for 5 min at the designated time intervals. DOX fluorescence in the supernatants was measured by fluorescence spectrometer.

Cell culture and animals

MCF-7 and MCF-7/ADR cells were kindly provided by Prof. Zhiping Zhang in School of Pharmacy, Huazhong University of Science and Technology (Wuhan, China). HepG2 and HepG2/ADM cells were kindly provided by Prof. Yin Wan in College of Life Science and Technology, Huazhong University of Science and Technology (Wuhan, China). MCF-7 and MCF-7/ADR cells were cultured in RPMI 1640 medium, and HepG2 and HepG2/ADM cells were cultured in DMEM medium containing 10% FBS, 100 U/mL penicillin G sodium and 100 µg/mL streptomycin sulfate at 37 °C in a humidified and 5% CO$_2$ incubator except adding 1 mg/mL DOX during MCF-7/ADR and HepG2/ADM cell culture.

Female nude mice (5 weeks, 16±2g) were provided by HUAFUKANG bioscience Co, LTD (Beijing, China). MCF-7/ADR tumor-bearing nude mice model was constructed by subcutaneously injecting 2×10^6 MCF-7/ADR cells into the right back of the nude mice. All animal experiments were approved by the Institutional Animal Care and Use Committee at Tongji Medical College, Huazhong

University of Science and Technology (Wuhan, China).

Cellular uptake

MCF-7, MCF-7/ADR, HepG2 or HepG2/ADM cells were cultured in a 12-well plate at a density of 2×10^5 cells per well. At 24 h after incubation, the cells were treated with DOX@PGNCs or DOX@pPGNCs at 10 μg/mL Au concentration for 12 h at pH 7.4, 6.5 or 6.0, respectively. Subsequently, the cells were washed with PBS and intracellular Au content was determined by graphite furnace atomic absorption spectrometry (AA-240FS, Agilent Technologies, Santa Clara, CA, USA).

NIR laser-induced intracellular drug release

MCF-7 and MCF-7/ADR cells were cultured in a 12-well plate at a density of 2×10^5 cells per well. At 24 h after incubation, the cells were treated with DOX@PGNCs or DOX@pPGNCs at 2 μg/mL DOX concentration for 4 h at pH 7.4 or 6.5, respectively, followed by irradiation with or without 808 nm NIR laser irradiation at a power density of 0.7 W/cm² for 5 min. Intracellular DOX content was determined by flow cytometry (FC500, Beckman Coulter, Fullerton, CA, U.S.A.) and confocal microscope. For confocal microscopic analysis, the cells were stained with 2.5 μg/mL DAPI for 15 min at 37 °C and then observed by an Olympus FV1000 confocal microscope (Tokyo, Japan).

In vitro cytotoxicity

MCF-7 or MCF-7/ADR cells were treated with free DOX, GNCs, PGNCs, pPGNCs, DOX@PGNCs or DOX@pPGNCs at DOX concentration of 1.2 μg/mL and Au concentration of 10 μg/mL at pH 7.4 or 6.5, respectively. At 24 h after treatment, the cells were washed with PBS and then irradiated with or without 808 nm NIR laser at a power density of 0.7 W/cm² for 5 min, followed by incubation for another 4 h. The cells were washed with PBS and then incubated in the media containing MTT solution (5 mg/mL) at 37 °C for another 4 h. The media were discarded and 150 μL DMSO was added to dissolve formazan crystals. The absorbance of formazan at 492 nm was measured by a Labsystems iEMS microplate reader (Helsinki, Finland).

In vivo biodistribution

MCF-7/ADR tumor-bearing nude mice were intravenously administrated with free DOX, DOX@PGNCs or DOX@pPGNCs at DOX dosage of 2.4 mg/kg, immediately followed with or without 808 nm laser irradiation at a power density of 0.7 W/cm² for 5 min at tumor sites. At 24 h after injection, the major organs including heart, liver, spleen, lung,

kidney and tumor were resected. These tissues were then washed with saline and homogenized with methanol and sonicated for 10 min at 45 °C. DOX content in the supernatants was measured by fluorescence spectrometer at the excitation wavelength of 488 nm and the emission wavelength of 560 nm.

In vivo tumor penetration

MCF-7/ADR tumor-bearing nude mice were intravenously administrated with free DOX, DOX@PGNCs or DOX@pPGNCs at the DOX dosage of 2.4 mg/kg, immediately followed with or without 808 nm laser irradiation at a power density of 0.7 W/cm² for 5 min at tumor sites. At 24 h after administration, the tumor tissues were harvested, washed with PBS and then frozen sectioned. The sections were stained with FITC-conjugated CD31 antibody at 37 °C for 30 min, washed with PBS and then observed by confocal microscope. The distribution of DOX fluorescence from blood vessels to tumor tissues was analyzed by software image J 1.45S.

In vivo photothermal effect

MCF-7/ADR tumor-bearing nude mice were intravenously administrated with PBS, DOX, GNCs, PGNCs, pPGNCs, DOX@PGNCs or DOX@pPGNCs at the Au dosage of 20 mg/kg., immediately followed with or without 808 nm laser irradiation at a power density of 0.7 W/cm² for 5 min at tumor sites. At 24 h after administration, the tumor tissues of mice were irradiated with 808 nm laser at a power density of 0.7 W/cm² for different time intervals. The temperature of the tumor tissues were detected by an FLIR E50 IR camera.

In vivo antitumor efficacy

MCF-7/ADR tumor-bearing nude mice were intravenously administrated with PBS, free DOX, GNCs, PGNCs, pPGNCs, DOX@PGNCs or DOX@pPGNCs at DOX dosage of 2.4 mg/kg and Au dosage of 20 mg/kg, immediately followed with or without 808 nm laser (0.7 W/cm²) irradiation for 5 min at tumor sites. The nude mice were further irradiated with or without 808 nm laser (0.7 W/cm²) for 5 min once every other day. Tumor sizes were monitored using a digital caliper every day and their volumes were calculated based on the formula: $V=(L \times W^2)/2$, where L and W are length and width of tumor, respectively. On day 15, the mice were sacrificed, and major organs including heart, liver, spleen, lung, kidney and tumor were excised, fixed and sliced for hematoxylin and eosin (H&E) staining.

Statistical analysis

All experiments were performed with at least three replicates. Student's *t* test was used to carry out the statistical analyses. $p < 0.05$ was considered significant.

Supplementary Material

Supplementary figures and tables.
http://www.thno.org/v09p3825s1.pdf

Competing Interests

The authors have declared that no competing interest exists.

References

1. Holohan C, Van Schaeybroeck S, Longley DB, Johnston PG. Cancer drug resistance: an evolving paradigm. Nat Rev Cancer. 2013; 13: 714–726.
2. Galluzzi L, Senovilla L, Vitale I, Michels J, Martins I, Kepp O, et al. Molecular mechanisms of cisplatin resistance. Oncogene. 2012; 31: 1869–1883.
3. Chen ZS, Tiwari AK. Multidrug resistance proteins (MRPs/ABCCs) in cancer chemotherapy and genetic diseases. FEBS J. 2011; 278: 3226–3245.
4. Xue X, Hall MD, Zhang Q, Wang PC, Gottesman MM, Liang XJ. Nanoscale drug delivery platforms overcome platinum-based resistance in cancer cells due to abnormal membrane protein trafficking. ACS Nano. 2013; 7: 10452–10464.
5. Yang T, Ke H, Wang Q, Tang Y1, Deng Y, Yang H, et al. Bifunctional tellurium nanodots for photo-induced synergistic cancer therapy. ACS Nano. 2017; 11: 10012–10024.
6. Deng Y, Huang L, Yang H, Ke H, He H, Guo Z, et al. Cyanine-anchored silica nanochannels for light-driven synergistic thermo-chemotherapy. Small. 2017; 13: 160274.
7. Li Y, Deng Y, Tian X, Ke H, Guo M, Zhu A, et al. Multipronged design of light-triggered nanoparticles to overcome cisplatin resistance for efficient ablation of resistant tumor. ACS Nano. 2015; 9: 9626–9637.
8. Li F, Yang H, Bie N, Xu Q, Yong T, Wang Q, et al. Zwitterionic temperature/redox-sensitive nanogels for near-infrared light-triggered synergistic thermo-chemotherapy. ACS Appl Mater Interfaces. 2017; 9: 23564–23573.
9. Zhang Z, Wang J, Nie X, Wen T, Ji Y, Wu X, et al. Near infrared laser-induced targeted cancer therapy using thermoresponsive polymer encapsulated gold nanorods. J Am Chem Soc. 2014; 136: 7317−7326.
10. Li L, ten Hagen TL, Schipper D, Wijnberg TM, van Rhoon GC, Eggermont AM, et al. Triggered content release from optimized stealth thermosensitive liposomes using mild hyperthermia. J Control Release. 2010; 143: 274−279.
11. Souslova T, Averill-Bates DA. Multidrug-resistant HeLa cells overexpressing MRP1 exhibit sensitivity to cell killing by hyperthermia: interactions with etoposide. Int J Radiat Oncol Biol Phys. 2004; 60: 1538–1551.
12. Hui L, Qin S, Yang L. Upper critical solution temperature polymer, photothermal agent, and erythrocyte membrane coating: an unexplored recipe for making drug carriers with spatiotemporally controlled cargo release. ACS Biomater Sci Eng. 2016; 2: 2127–2132.
13. Piao JG, Wang L, Gao F, You YZ, Xiong Y, Yang L. Erythrocyte membrane is an alternative coating to polyethylene glycol for prolonging the circulation lifetime of gold nanocages for photothermal therapy. ACS Nano. 2014; 8: 10414–10425.
14. Wang Z, Chen Z, Liu Z, Shi P, Dong K, Ju E, et al. A multi-stimuli responsive gold nanocage-hyaluronic platform for targeted photothermal and chemotherapy. Biomaterials. 2014; 35: 9678–9688.
15. Sun T, Wang Y, Wang Y, Xu J, Zhao X, Vangveravong S, et al. Using SV119-gold nanocage conjugates to eradicate cancer stem cells through a combination of photothermal and chemotherapies. Adv Healthc Mater. 2014; 3: 1283–1291.
16. Xu Q, Wan J, Bie N, Song X, Yang X, Yong T, et al. A biomimetic gold nanocages-based nanoplatform for efficient tumor ablation and reduced inflammation. Theranostics. 2018; 8: 5362–5378.
17. Skrabalak SE, Chen J, Au L, Lu X, Li X, Xia Y. Gold nanocages for biomedical applications. Adv Mater. 2007; 19: 3177–3184.
18. Au L, Zheng D, Zhou F, Li ZY, Li X, Xia Y. A quantitative study on the photothermal effect of immuno gold nanocages targeted to breast cancer cells. ACS Nano. 2008; 2: 1645–1652.
19. Chen J, Wang D, Xi J, Au L, Siekkinen A, Warsen A, et al. Immuno gold nanocages with tailored optical properties for targeted photothermal destruction of cancer cells. Nano Lett. 2007; 7: 1318–1322.
20. Li W, Cai X, Kim C, Sun G, Zhang Y, Deng R, et al. Gold nanocages covered with thermally-responsive polymers for controlled release by high-intensity focused ultrasound. Nanoscale. 2011; 3: 1724–1730.
21. Yavuz MS, Cheng Y, Chen J, Cobley CM, Zhang Q, Rycenga M, et al. Gold nanocages covered by smart polymers for controlled release with near-infrared light. Nat Mater. 2009; 8: 935–939.
22. Lammers T, Kiessling F, Hennink WE, Storm G. Drug targeting to tumors: principles, pitfalls and (pre-) clinical progress. J Control Release. 2012; 161: 175–187.
23. Andreev OA, Karabadzhak AG, Weerakkody D, Andreev GO, Engelman DM, Reshetnyak YK. pH (low) insertion peptide (pHLIP) inserts across a lipid bilayer as a helix and exits by a different path. Proc Natl Acad Sci U S A. 2010; 107: 4081–4086.
24. Tapmeier TT, Moshnikova A, Beech J, Allen D, Kinchesh P, Smart S, et al. The pH low insertion peptide pHLIP variant 3 as a novel marker of acidic malignant lesions. Proc Natl Acad Sci U S A. 2015; 112: 9710–9715.
25. Lutz JF, Akdemir O, Hoth A. Point by point comparison of two thermosensitive polymers exhibiting a similar LCST: is the age of poly(NIPAM) over? J Am Chem Soc. 2006; 128: 13046−13047.
26. Vancoillie G, Frank D, Hoogenboom R. Thermoresponsive poly(oligo ethylene glycol acrylates). Prog Polym Sci. 2014; 39: 1074−1095.
27. Yang H, Wang Q, Chen W, Zhao Y, Yong T, Gan L, et al. Hydrophilicity/hydrophobicity reversable and redox-sensitive nanogels for anticancer drug delivery. Mol Pharm. 2015; 12: 1636−1647.
28. Yang H, Wang Q, Li Z, Li F, Wu D, Fan M, et al. Hydrophobicity-adaptive nanogels for programmed anticancer drug delivery. Nano Lett. 2018; 18: 7909–7918.
29. Barenholz Y. Doxil®-the first FDA-approved nano-drug: lessons learned. J Control Release. 2012; 160: 117–134.
30. Chabner BA, Roberts TG Jr. Timeline: chemotherapy and the war on cancer. Nat Rev Cancer 2005; 5: 65−72.
31. Huang W, Lang Y, Hakeem A, Lei Y, Gan L, Yang X. Surfactin-based nanoparticles loaded with doxorubicin to overcome multidrug resistance in cancers. Int J Nanomedicine. 2018; 13: 1723−1736.
32. Yong T, Hu J, Zhang X, Li F, Yang H, Gan L, et al. Domino-like intercellular delivery of undecylenic acid-conjugated porous silicon nanoparticles for deep tumor penetration. ACS Appl Mater Interfaces. 2016; 8: 27611−27621.
33. Jain RK, Stylianopoulos T. Delivering nanomedicine to solid tumors. Nat Rev Clin Oncol. 2010; 7: 653−664.
34. Minchinton AI, Tannock IF. Drug penetration in solid tumours. Nat Rev Cancer. 2006; 6: 83−92.
35. Skrabalak SE, Au L, Li X, Xia Y. Facile synthesis of Ag nanocubes and Au nanocages. Nat. Protoc. 2007; 2: 2182–2190.
36. Wan J, Geng S, Zhao H, Peng X, Zhou Q, Li H, et al. Doxorubicin-induced co-assembling nanomedicines with temperature-sensitive acidic polymer and their in-situ-forming hydrogels for intratumoral administration. J Control Release. 2016; 235: 328–336.